Catal Lett (2012) 142:224–230
DOI 10.1007/s10562-011-0762-4

Optimization of Opto-Electrical and Photocatalytic Properties of SnO_2 Thin Films Using Zn^{2+} and W^{6+} Dopant Ions

Alexandru Enesca · Luminita Andronic · Anca Duta

Received: 17 September 2011 / Accepted: 19 December 2011 / Published online: 6 January 2012
© Springer Science+Business Media, LLC 2012

Abstract A series of Zn^{2+} and W^{6+} doped tin oxide (SnO_2) thin films with various dopant concentrations were prepared by spray pyrolysis deposition, and were characterized by X-ray diffraction, atomic force microscopy, contact angle, absorbance, current density–voltage (J–V) and photocurrent measurements. The results showed that W^{6+} doping can prevent the growth of nanosized SnO_2 crystallites. When Zn^{2+} ions were used, the crystallite sizes were proved to be similar with the undoped sample due to the similar ionic radius between Zn^{2+} and Sn^{4+}. Regardless of the dopant ions' type or concentration, the surface energy has a predominant dispersive component. By using Zn^{2+} dopant ions it is possible to decrease the band gap value (3.35 eV) and to increase the electrical conductivity. Photocatalytic experiments with methylene blue demonstrated that with zinc doped SnO_2 films photodegradation efficiencies close to 30% can be reached.

Keywords Thin films · Dopant · Opto-electric · Photocatalytic

1 Introduction

Tin oxide (SnO_2) is a versatile wide band gap (3.6 eV at 300 K) *n*-type semiconducting oxide with a wide variety of applications. Due to its electrical and optical properties (transparent for visible and reflective for infrared light) and good chemical and mechanical stability, it is commonly used in oxidation catalysis, gas sensing, transparent conducting oxides and opto-electronic devices [1–3]. The properties of SnO_2 nanostructures can be enhanced in several ways such as impurity doping, polymeric additives and annealing [4, 5]. However, the stoichiometric SnO_2 leads to low performance because of the low intrinsic carrier density and mobility, mainly as a result of the double ionized vacancies serving as donors [6–8].

The use of dopants to control surface properties of SnO_2 thin films allows obtaining nanostructures with tailored and predictable macroscopic properties [9–11], and represents a promising way towards obtaining advanced materials with application in solar energy conversion (photovoltaic, photocatalytic and photoelectrolytic systems) [12–14].

In recent years scientists are investigating many semiconductor-assisted photocatalysts such as TiO_2, ZnO, SnO_2,WO_3, etc. [15–17] due to the capacity of the semiconductors to degrade a large number of organic compounds in aqueous systems, in particulary dyes from textile wastewaters [18]. It is of great importance to study the effects of metals doping in SnO_2 on the electron transfer and the metal modification mechanisms relating to the surface oxygen vacancies in order to find an effective method to enhance the photocatalytic activity [19, 20].

In the present work the influence of Zn^{2+} and W^{6+} dopant ions on different target properties such as morphology, surface tensions, band gap, electrical conductivity and photocatalytic activity was investigated. Tailoring the physical properties and adding new functionalities to the existing semiconductors by altering the structure, composition, and particle/grain size are the new approaches in advancing the current applications of semiconductor materials. The preparation of these materials at nanoscopic or mesoscopic scale supports the increase of the surface-to-volume ratio, with consequences on the structure and other physical properties.

A. Enesca (✉) · L. Andronic · A. Duta (✉)
Renewable Energy Systems and Recycling Department, Transilvania University of Brasov, Eroilor 29 Street, 500036 Brasov, Romania
e-mail: aenesca@unitbv.ro

A. Duta
e-mail: a.duta@unitbv.ro

The dopant ions were chosen according to the tin oxidation state, considering the possibility of increasing the number of a certain charge carrier (*n* or *p* conductivity). Photocatalytic experiments with methylene blue as a reference substance were performed to investigate the possibility for organic pollutant removal from wastewater.

2 Experimental

2.1 Precursor Preparation and Deposition Parameters

Five sample types were prepared by SPD using microscopic glass (Heinz Herenz) and FTO (fluorine doped SnO_2, SnO_2, coated glass—Libbey Owens Ford TEC 20/2.5 nm) as substrate for thin films deposition. The deposition temperature was 450 °C and the carrier gas was air at 1.4 bars. Samples of 2 × 2 cm^2 microscopic glass were cleaned by successive immersion in ethanol and acetone using an ultrasonic bath. The precursor solution was prepared by mixing 0.05 M tin chloride ($SnCl_4$, 99.99%, Alfa Aesar) and ethanol (C_2H_5OH, 99.99%, Alfa Aesar) with 0.05 M zinc chloride ($ZnCl_2$, 99.99%, Alfa Aesar) or 0.05 M tungsten chloride (WCl_6, 99.99%, Alfa Aesar) in different atomic weight percentage (Table 1). The doping concentration was limited to avoid ternary compound formation.

As post-deposition treatment, the samples were annealed at 500 °C for 6 h.

2.2 Photocatalysis Experiments

The photodegradation reactor consists of a static cylindric flask, open to air. Three F18W/T8 black light tubes (Philips) (UVA light, typically 340–400 nm, $\lambda_{max} = 365$ nm), placed annular to the photoreactor were used for photocatalysis. The system work in static regime and is totally closed during the experiments, [21, 22].

The pollutant dye tested in this work was 0.0125 mM methylene blue (99.8%, Merck) prepared by dissolving the powder in ultra pure water (Direct-Q3 Water Purification System). Absorbance measurements (Perkin Elmer Lambda 25 UV/VIS) were recorded in the range of 200–800 nm; the photocatalytic efficiency was calculated based on the calibration curve, at the maximum absorption wavelength experimentally registered at $\lambda = 665$ nm. Each sample (2 × 2 cm^2) is inserted into a 25 mL quartz glass and let 1 h in dark. Before the UV–VIS light is on (second step which take 6 h) the dye solution concentration is tested and calibrated (at 0.0125 mM) due to the absorption process that occur in the first step.

Table 1 Dopant ions type and concentrations

Sample names	Dopant source	Dopant ions	Atomic ratio (wt%)
Sn	–	–	–
Sn_0.25Zn	$ZnCl_2$	Zn^{2+}	0.25
Sn_0.5Zn	$ZnCl_2$	Zn^{2+}	0.5
Sn_0.25W	WCl_6	W^{6+}	0.25
Sn_0.5W	WCl_6	W^{6+}	0.5

2.3 Film Characterization

The XRD analysis (Bruker D8 Discover Advanced Diffractometer) was performed using locked-couple technique with 0.002 degree scan step and 0.01 s/step. The morphology of the nanocomposite structure was studied using an Atomic Force Microscope (AFM, NT-MDT model BL222RNTE). The images were taken in semicontact mode with Si-tips (NSG10, force constant 0.15 N/m, tip radius 10 nm).

Static contact angle measurements, with the sessile drop method were recorded and analyzed using an OCA-20 Contact Angle-meter (DataPhysics Instruments).

The current–voltage curves and photocurrent measurements were done using a multichannel potentiostat (PAR Instruments, model HM 8143) with a frequency analyzer, a monochromator (Acton, SpectraPro 2150i) and a UV–VIS light source (Oriel, model 7123). The current–voltage analyses were made using two graphite contacts: one contact on the FTO substrate (used for the applied voltage) and the second on the top of the layers (used as current receptor). Both contacts were placed at equal distance (1.5 cm) on each sample. Absorbance and reflectance measurements were recorded using a UV–VIS spectrophotometer (Perkin Elmer Lambda 25 UV/VIS).

3 Results and Discussions

3.1 Crystalline Structure and Morphology

The diffractions data (Fig. 1) show the formation of tetragonal SnO_2 in doped and undoped samples. Several papers [23–25] report the formation of stannous oxide (SnO) simultaneously with the formation of SnO_2. To prevent this inconvenience, the Sn sample was annealed at 500 °C, which can explain the formation of the higher oxidation state compound. There is no evidence of crystalline secondary metal oxides (ZnO or WO_3) or ternary compounds formation, confirming that the doping ions were inserted in the host lattice. The doping process can theoretically follow various paths but the defects formation is supported by the thermodynamically favored reactions:

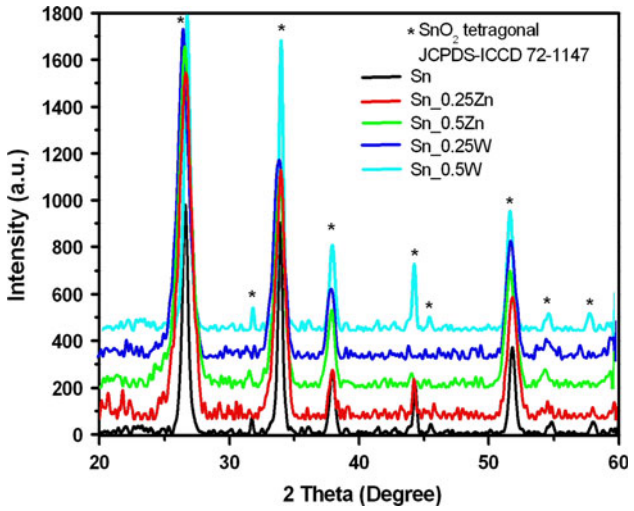

Fig. 1 XRD patterns of doped SnO_2 layers

the development of the minimum number of defects with the lowest charge. These are described by the following equations (the Kröger–Vink notation was used):

$$SnO_2 \xrightarrow[[ZnO]]{} Zn''_{Sn} + V_O^{\bullet\bullet} + O_O^x, \text{ for } Zn^{2+} \text{ dopant} \quad (1)$$

$$SnO_2 \xrightarrow[[WO_3]]{} W_{Sn}^{\bullet\bullet} + O_i'' + 2O_O^x, \text{ for } W^{6+} \text{ dopant} \quad (2)$$

according to Fig. 1, the samples showed preferred orientation along the (110) plane. Secondary reflections were also observed along the planes (101). The micro-strains values where determined by dedicated Bruker software (EVA Diffrac Plus Evaluation) which measure and compare the deviation from the ideal lattice size. Considering the (110) and (101) planes, the crystallite size values, D, given in Table 2 were calculated with the Scherrer formula from the full-width-half-maximum (FWHM) values obtained from the XRD-data shown in Fig. 1.

$$D = \frac{K\lambda}{FWHM \cdot \cos\theta} = \frac{0.9 \cdot \lambda}{FWHM \cdot \cos\theta}. \quad (3)$$

Many results have shown that several dopants (Co, Fe and Cu) can lead to an increase in the SnO_2 surface area by reducing the grain size and crystallinity [26]. A similar observation can be made for the W^{6+} doping ions (Table 2) which act as inhibitors in the crystal growth especially when the dopant concentration reaches 0.5 wt%. The Zn^{2+} replace the Sn^{4+} ions in the crystal lattice due to comparable ionic radius ($r_{Zn2+} = 0.074$ and $r_{Sn4+} = 0.071$ nm) without significant modification of the crystallite size and micro strain. Differences in the micro strain values are present in the case of the W^{6+} dopant where the ionic radius ($r_{W6+} = 0.065$ nm) is slightly different as compared to Sn^{4+}.

Table 2 Network parameters and surface roughness

Sample	Crystallite size (Å) (110)	Crystallite size (Å) (101)	Micro-strains (ε)	Roughness (nm)
Sn	272.4	338.9	0.0027	2.83
Sn_0.25Zn	289.1	344.2	0.0021	5.28
Sn_0.5Zn	394.9	359.1	0.0023	10.47
Sn_0.25W	191.3	293.4	0.0032	3.85
Sn_0.5W	191.9	301.3	0.0039	3.89

The AFM images (Fig. 2) were made on $5 \times 5\ \mu m^2$ which is considered representative for the entire surface. The roughness analysis are made by dedicated AFM software (NTEGRA) considering the basic statistical parameters for the source object (2D function) and forms the function values distribution density histogram. The source object (source image) is a discrete two-dimensional function $Z(X_i, Y_j)$ with a certain minimal step in Z-direction. Correspondingly on the histogram the values of Z function are set on X axis with a certain step. With Z_Step parameter value of 1 this step is equal to the step of the source function in Z-direction. As the value of Z_Step parameter increases, the step in X-direction increases proportionally. On the histogram for each value of X (i.e. the value of the source function) a certain number of points is set in Y-direction with the values ranging from Z to Z + Z_step. $Z_{ij} = Z(X_i, Y_j)$ is a discrete function, set on XY plane, whereas is the number of points on X, Y axes. The results indicate a homogeneous morphology with roughness that varies between 2.83 and 3.89 nm for undoped and W^{6+} doped samples. On the contrary, the Zn^{2+} doped samples present large non-uniformity as a consequence of the different aggregates size that are formed during the annealing treatment. Also, the roughness of Zn^{2+} doped samples increases up to 10.47 nm. Compared with the undoped samples, the presence of different doped ions has a significant impact on the layer morphology and it increases the active surface area necessary for photocatalytic processes.

The contact angle measurements (Fig. 3) were performed to investigate the influence of the morphology and the crystallinity on the films surface properties. Glycerol (with a polar component of the energy $\sigma^p = 41.50$ mN/m and a dispersion component of the energy $\sigma^d = 21.20$ mN/m) was used to evaluate the contact angle variation in time (180 s). The undoped sample and Zn^{2+} doped samples present an absorption rate that varies from 0.08°/s (for sample Sn) to 0.1°/s (for sample Sn_0.5Zn). High values of the absorption rate are usually present in porous samples (Zn^{2+} doped samples). On the contrary, the W^{6+} doped sample reaches the saturation point in the first 20 s (0.02°/s absorption rate) as a consequence of the morphology

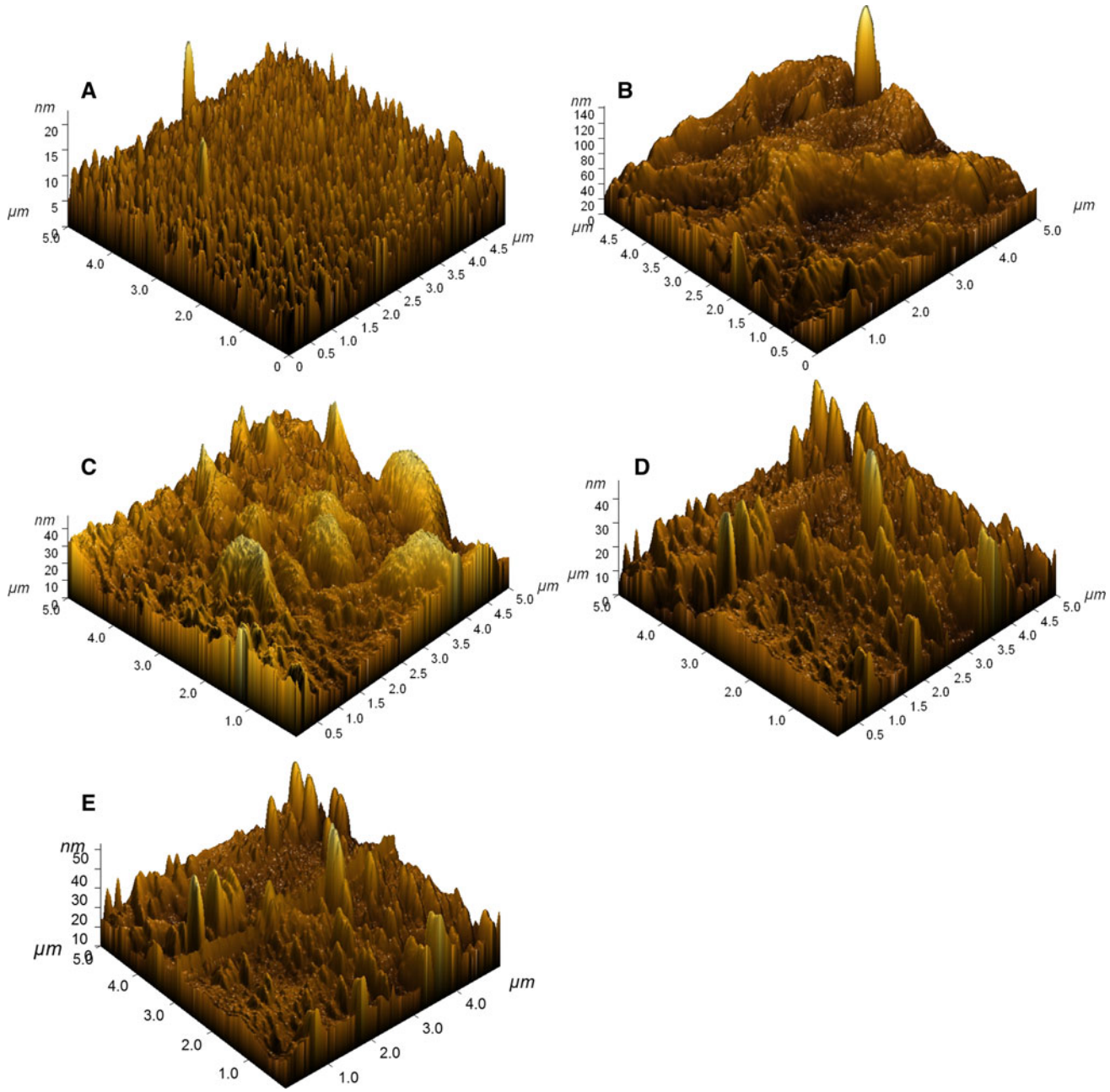

Fig. 2 The AFM images of the samples **a** Sn, **b** Sn_0.25Zn, **c** Sn_0.5Zn, **d** Sn_0.25W and **e** Sn_0.5W

densification and hydrophobic character induced by the dopant ions. However, the photocatalytic application requires surfaces with hydrophilic character such as the Sn_0.25Zn and Sn_0.5Zn samples.

Using the Fowkes equation (Eq. 4), that includes the dispersed and polar components of the liquid–solid interface, values of the surface energy were calculated for each sample and are presented in Table 3.

According to Fowkes:

$$\sigma_{LV}(1+\cos\theta) = 2\left[\left(\sigma_{LV}^{p}\sigma_{SV}^{p}\right)^{\frac{1}{2}} + \left(\sigma_{LV}^{d}\sigma_{SV}^{d}\right)^{\frac{1}{2}}\right]. \quad (4)$$

where σ_{LV}^{p}, σ_{LV}^{d}, σ_{SV}^{p}, σ_{SV}^{d} are polar and dispersed components of the liquid- and solid-surface energies, respectively.

The surface energy investigation shows that all samples have a predominant dispersive component. This behavior is more evident for Zn^{2+} doped samples and can be explained by the surface non-homogeneity, which increases the high surface energy areas (located mostly at the grain boundaries). The W^{6+} doped samples present also a polar component due to the slightly acid character induced by the tungsten ions.

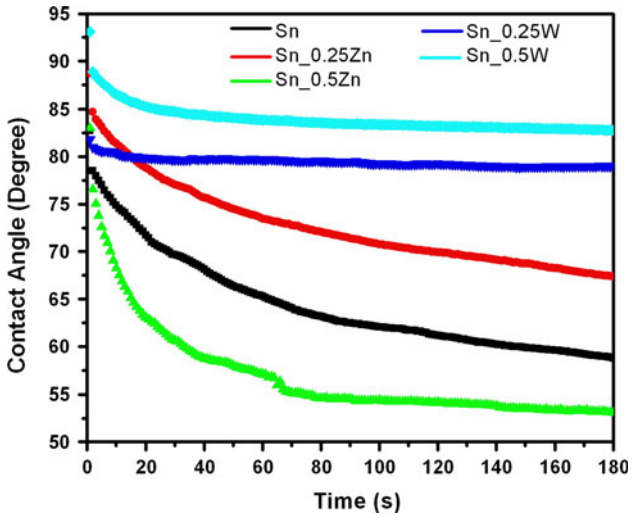

Fig. 3 Contact angle measurements with glycerine

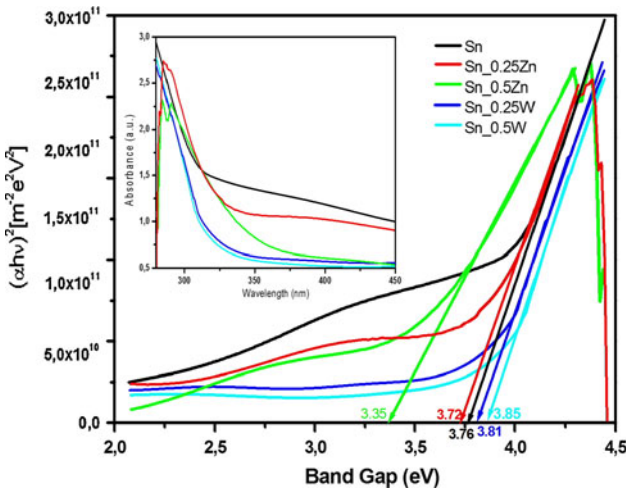

Fig. 4 Band gap energy and the related absorbance spectra

Table 3 The surface energy values of the samples

Sample	Surface energy	Dispersion component	Polar component
Sn	59.42	59.37	0.04
Sn_0.25Zn	73.12	72.48	0.63
Sn_0.5Zn	68.61	68.00	0.61
Sn_0.25W	31.09	27.13	3.96
Sn_0.5W	27.11	23.26	3.85

The calculation made following the contact angle measurement shows that, depending on the dopant concentration, the surface energy tensions varies and maintains a predominant dispersive component.

3.2 Electrical and Opto-Electrical Properties

Using the absorbance spectra (Fig. 4) the band gap energy were evaluated considering the influence of the doping ions on the energetic levels. Lower band gap values (compared to the undoped sample) were obtained for tin based sample, with direct influence on the layer conductivity. The lowest values (3.35 eV) correspond to the Sn_0.5Zn sample showing that 0.5 wt% represents the optimum concentration. The insertion of W^{6+} ions increases the band gap values up to 3.85 eV (for sample Sn_0.5W) which makes the layers highly electrical resistive.

The current density–voltage curves (Fig. 5) confirms the results obtained from the band gap evaluation. SnO_2 is known as an oxygen-deficient *n*-type semiconductor that can be modified depending on the doping ions, and during the annealing treatment the holes concentration increases according to the following equation:

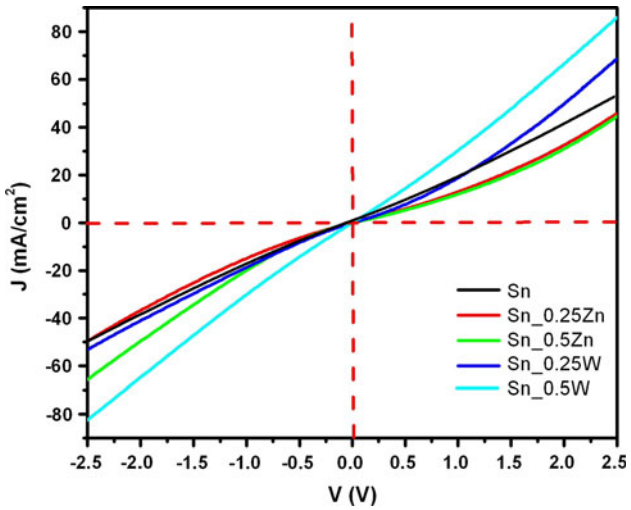

Fig. 5 Current density–voltage curves for undoped and doped SnO_2 layers

$$V_O^{\bullet\bullet} + 1/2O_2 \rightarrow O_O^x + 2h^{\bullet} \quad (5)$$

the Zn^{2+} dopant ions increase the concentration of oxygen vacancies that is partially reduced during the annealing treatment, when positive carrier charges (holes) are formed. In this case, it is even possible to induce *p*-type conductivity into the materials if the proper dopant concentration is used. Consequently, the highest electrical conductivity was obtained for the Sn_0.5Zn sample. The W^{6+} dopant induces two concurrent processes: recombination and generation of donor carrier charge. Regardless of the W^{6+} dopant concentration, the electrical resistivity significantly increases compared with the undoped and Zn^{2+} doped samples.

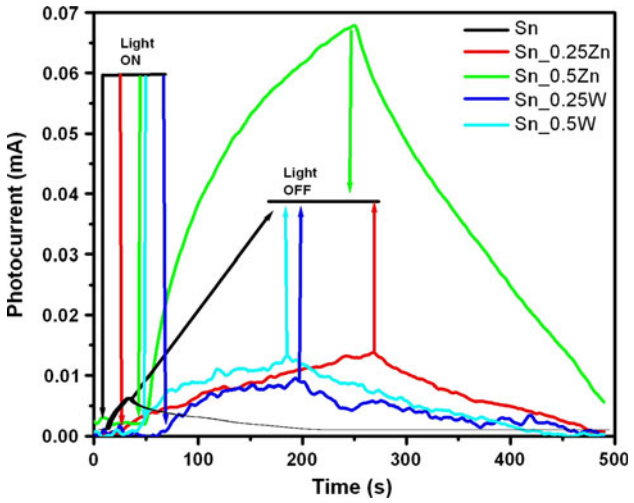

Fig. 6 Photocurrent measurements with a bias of 0.05 V

The photosensitivity properties of the samples were tested by measuring the photo-generated current (Fig. 6) during the irradiation. The undoped sample presents the lowest photocurrent values. By using dopant ions, it is possible to increase the photosensitive properties by shifting the spectral range close to the visible light. The possibility to absorb more photons by the photo-catalyst is a key factor for improving the pollutant photo-degradation. Consequently, the higher photocurrent values correspond to the zinc doped samples, showing that the process of choosing the right doping ions and concentration will improve the opto-electrical properties of the layer. The tungsten ions will give better photosensitive properties, compared to the undoped sample, but the photocurrent presents non-stable behavior in time. The photocurrent stability is reduced in doped sample due to the presence of the higher micro-strain values and the charge recombination induced by defects.

3.3 Photocatalysis Efficiency

The photodegradation efficiency was evaluated with the following relation:

$$\eta = [(A_0 - A)/A_0] * 100 \quad (6)$$

where A_0 represents the initial absorbance of the dye solution and A represents the absorbance of the dye solution after irradiation time t (the measurements were made hourly for 6 h).

The experiments with methylene blue solution show (Fig. 7) that the Sn_0.25Zn sample has a higher photocatalytic activity with an efficiency amounting up to 12%. Half of this value was recorded for the next samples: Sn, Sn_0.5Zn and Sn0.5W. When hydrogen peroxide is added in the methylene blue solution, the photocatalytic efficiency increased up to 30% (for the sample Sn_0.25Zn)

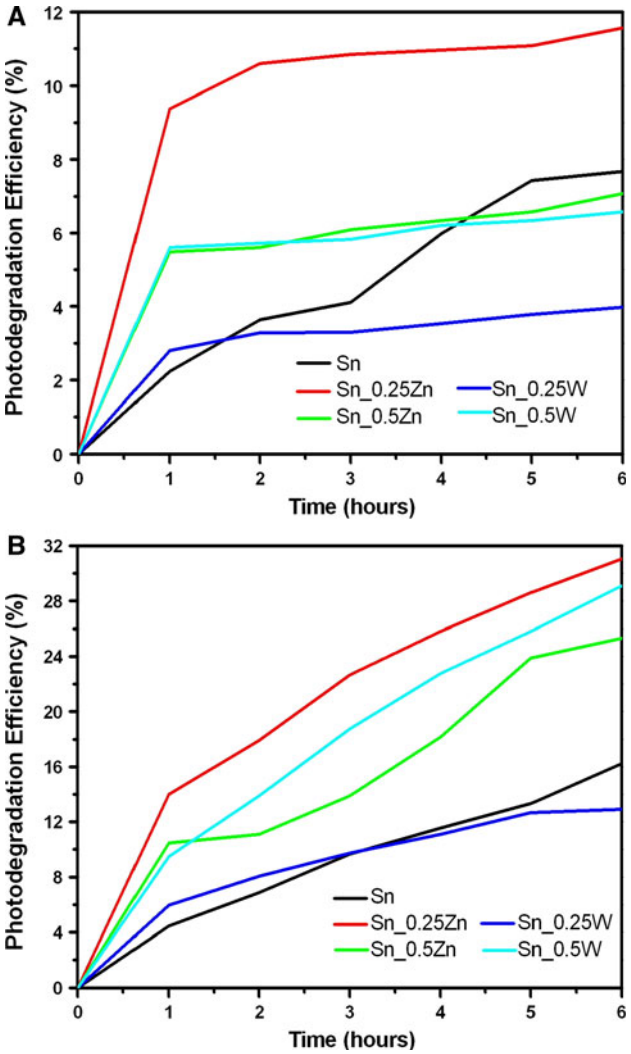

Fig. 7 Photocatalysis efficiency in methylene blue solution with **a** water and **b** water and hydrogen peroxide

and 28% (for sample Sn_0.5W). The hydrogen peroxide improves the oxidation process by increasing the number of Brønsted base sites. Many Brønsted acids dissociate on oxide surfaces, causing protonation of the surface oxygen anions, and adsorption of the conjugated base of the acid to metal cations at the surface [27, 28]. The key requirement for the dissociative adsorption is thus the availability of pairs of under-coordinated metal cations and surface base sites (oxygen). The protonation processes are responsible for degradation of the organic molecules (dye in this case) and they improve the photocatalytic efficiency.

4 Conclusions

Undoped and doped SnO_2 thin films were obtain by employing the spray pyrolysis deposition (SPD) using dopants in different atomic weight percentage. Regardless

of the doping ions type (Zn^{2+} or W^{6+}) or concentration, the diffraction analysis shows the formation of tetragonal SnO_2 without other secondary products. Due to the similarity between the Sn^{4+} and Zn^{2+} ionic radii there are no significant differences on the crystallite size and network stress. On the contrary, the tungsten ions act as crystalline inhibitors and reduce the crystallite size values.

A regular morphology was recorded for undoped and W^{6+} doped samples due to the uniform distribution of the nucleation sites on the substrate surface. The Zn^{2+} doped samples present non-homogeneous morphology (roughness of 10.47 nm for Sn_0.5Zn sample) as a consequence of aggregates formation with different size. All samples present a predominant dispersive component of the surface energy.

Several modifications of the opto-electrical properties were observed depending on the dopant ions. By inserting Zn^{2+} ions, it is possible to decrease the band gap values (3.35 eV) and to increase the electrical conduction. The W^{6+} ions act differently and increase the SnO_2 band gap and the electrical resistivity.

One of the major applications of these layers is represented by the removal of organic pollutants form wastewater. The SnO_2 layer doped with 0.25 wt% Zn^{2+} has a photocatalytic efficiency of $\sim$30% as compared with the undoped sample where 15% is the maximum value. Until recently, SnO_2 was considered a poor photocatalytic material, and the possibility of improving this property by inserting dopant ions into the network seems highly promising.

Acknowledgments This paper is supported by the Sectoral Operational Programme Human Resources Development (SOP HRD), financed from the European Social Fund and by the Romanian Government under the contract number POSDRU ID59323.

References

1. Liu X, Zhang J, Guo X, Wu S, Wang S (2011) Sens Actuator B 152:162
2. Fu C, Wang J, Yang M, Su X, Xu J, Jiang B (2011) J Non Cryst Solids 357:1172
3. Navgire ME, Lande MK, Gambhire AB, Rathod SB, Aware DV, Bhitre SR (2011) B Mater Sci 3:535
4. Kalygina VM, Zarubin AN, YeP N, Novikov VA, Petrova YS, Tolbanov OP, Tyazhev AV, Yaskevich TM (2011) Semiconductors 45:1097
5. Liu S, Ding W, Chai W (2011) Phys B 406:2303
6. Choudhury B, Choudhury A, Maidul AKM, Alagarsamy P, Mukherjee M (2011) J Magn Magn Mater 323:440
7. Mishra AK, Sinha TP, Bandyopadhyay S, Das D (2011) Mater Chem Phys 125:252
8. Giribabu L, Singh VK, Srinivasu M, Kumar CV, Reddy VG, Soujnya Y, Reddy PY (2011) J Chem Sci 123:371
9. Stambolova I, Blaskov V, Vassilev S, Shipochka M, Dushkin C (2010) J Alloy Compd 489:257
10. Sathyaseelan B, Senthilnathan K, Alagesan T, Jayavel R, Sivakumar K (2010) Mater Chem Phys 124:1046
11. Ding X, Zeng D, Xie C (2010) Sens Actuator B 149:336
12. Wei W, Dai Y, Guo M, Zhang Z, Huang B (2010) J Solid State Chem 183:3073
13. Klamchuen A, Yanagida T, Kanai M, Nagashima K, Oka K, Kawai T, Suzuki M, Hidaka Y, Kai S (2010) J Cryst Growth 312:3251
14. Soitah TN, Yang C, Sun L (2010) Mat Sci Semicon Proc 13:25
15. Habibi MH, Nasr-Esfahani M (2007) Dyes Pigments 75:714
16. Chan SH, Wu TY, Juan JC, Yang C (2011) J Chem Technol Biot 86:1130
17. Rehman S, Ullah R, Butt AM, Gohar ND (2009) J Hazard Mater 170:560
18. Oller I, Malato S, Sánchez-Pérez JA (2011) Sci Total Environ 409:4141
19. Epifani M, Alvisi M, Mirenghi L, Leo G, Siciliano P, Vasanelli L (2001) J Am Ceram Soc 84:48
20. Korotcenkov G, Han SD (2009) Mater Chem Phys 113:756
21. Andronic L, Manolache S, Duta A (2008) J Nanosci Nanotechnol 8:728
22. Andronic L, Hristache B, Enesca A, Visa M, Duta A (2009) Environ Eng Manag J 8:747
23. Batsanov SS (2011) J Struct Chem 52:602
24. Goldsmith S, Çetinörgü E, Boxman RL (2009) Thin Solid Films 517:5146
25. Xiangping C, Jianyu L, Zhentao Z, Huanan D, Boquan L, Qiming Y (2010) Mater Res Bull 45:2006
26. Ahmed AS, Muhamed SM, Singla ML, Tabassum S, Naqvi AH, Azam A (2011) J Lumin 131:1–6
27. Enesca A, Andronic L, Duta A (2009) Environ Eng Manage J 8:753
28. Enesca A, Duta A (2008) Phys Status Solidi C 5:3499